PCCP

Multiresolution quantum chemistry in multiwavelet bases: Excited states from time-dependent Hartree-Fock and density functional theory via linear response

Journal:	*Physical Chemistry Chemical Physics*
Manuscript ID:	CP-ART-12-2014-005821.R2
Article Type:	Paper
Date Submitted by the Author:	09-Feb-2015

Complete List of Authors:	Yanai, Takeshi; Institute for Molecular Science, Department of Theoretical and Computational Molecular Science Fann, George; Oak Ridge National Laboratory, Computer Science and Mathematics Division Beylkin, Gregory; University of Colorado at Boulder, Department of Applied Mathematics Harrison, Robert; Stony Brook University, Institute for Advanced Computational Science

Physical Chemistry Chemical Physics
CREATED USING THE RSC LaTeX PCCP ARTICLE TEMPLATE – SEE www.rsc.org/electronicfiles FOR DETAILS
ARTICLE TYPE www. rsc.org/xxxxxx | XXXXXXXX

Multiresolution quantum chemistry in multiwavelet bases: Excited states from time-dependent Hartree-Fock and density functional theory via linear response

Takeshi Yanai,*[a] George I. Fann,[b] Gregory Beylkin,[c] Robert J. Harrison*[d,e]

Received Xth XXXXXXXXXX 20XX, Accepted Xth XXXXXXXXX 20XX
First published on the web Xth XXXXXXXXXX 200X
DOI: 10.1039/b000000x

A fully numerical method for the time-dependent Hartree-Fock and density functional theory (TD-HF/DFT) with the Tamm-Dancoff (TD) approximation is presented in a multiresolution analysis (MRA) approach. From a reformulation with effective use of the density matrix operator, we obtain a general form of the HF/DFT linear response equation in the first quantization formalism. It can be readily rewritten as an integral equation with the bound-state Helmholtz (BSH) kernel for the Green's function. The MRA implementation of the resultant equation permits excited state calculations without virtual orbitals. The integral equation is efficiently and adaptively solved using a numerical multiresolution solver with multiwavelet bases. Our implementation of the TD-HF/DFT methods is applied for calculating the excitation energies of H_2, Be, N_2, H_2O, and C_2H_4 molecules. The numerical errors of the calculated excitation energies converge in proportion to the residuals of the equation in the molecular orbitals and response functions. The energies of the excited states at a variety of length scales ranging from short-range valence excitations to long-range Rydberg-type ones are consistently accurate. It is shown that the multiresolution calculations yield the correct exponential asymptotic tails for the response functions, whereas those computed with Gaussian basis functions are too diffuse or decay too rapidly. We introduce a simple asymptotic correction to the local spin-density approximation (LSDA) so that in the TDDFT calculations, the excited states are correctly bound.

1 Introduction

In a series of papers[1–3], we described a practical multiresolution method using multiwavelet bases for the all-electron Hartree-Fock (HF) and Kohn-Sham (KS) equations for quantum chemical calculations. These studies employed and extended the approach described in Ref.[4] for the solution of the integral and partial differential equations. In this paper, we describe a multiresolution numerical solver that performs the linear response calculations for excitation energies using the time-dependent Hartree-Fock and density functional theory.

Determining molecular properties, such as the excitation energies, transition moments, frequency-dependent polarizabilities, and other spectroscopic parameters, is an important subject in computational quantum chemistry. A central task of the property calculations is the determination of molecular response functions associated with molecular properties. In the response theory, the response is formulated as a time-dependent perturbation[5]. The linear response method for the HF theory is derived from the time-dependent HF (TDHF) equation[6,7]. The TDHF method is widely used in nuclear physics, where it is known as the "random-phase approximation" (RPA)[8]. The Tamm-Dancoff (TD) approximation to the TDHF method gives an equivalent of the configuration interaction with single substitutions (CIS) method, known as the simplest quantum chemistry approach to excited states. These methods are based on the single excitation picture and essentially neglect electron correlation; therefore, they provide accuracy to the mean-field level.

Over the past decades, the time-dependent density functional theory (TDDFT) has been actively studied and well established to determine the response properties on the basis of the Kohn-Sham theory[9–18]. With the aid of modern computational algorithms, the TDDFT method has become a widely used computational approach that can predict molecular properties efficiently and reliably. The predictions of the TDDFT method are surprisingly accurate relative to the results calculated by the TDHF method, while the computational complexity and execution costs of these methods are almost equivalent. The TDDFT with the TD approximation (TDDFT/TD)

[a] *Department of Theoretical and Computational Molecular Science, Institute for Molecular Science, Okazaki, Aichi 444-8585, Japan;* [b] *Computer Science and Mathematics Division, Oak Ridge National Laboratory, Oak Ridge, Tennessee 37831, USA;* [c] *Department of Applied Mathematics, University of Colorado at Boulder, 526 UCB, Boulder, CO 80309-0526, USA;* [d] *Institute for Advanced Computational Science, Stony Brook University, Stony Brook, New York 11794, USA;* [e] *Computational Science Center, Brookhaven National Laboratory, Upton, New York 11973, USA; E-mail: yanait@ims.ac.jp; Robert.Harrison@stonybrook.edu.*

was proposed and examined by Hirata and Head-Gordon[16,17]. They concluded that the performance of the TDDFT/TD is in many cases comparable to that of TDDFT without the TD approximation. Recent advances in the development of exchange-correlation functionals have clarified and improved the previously poor description of Rydberg states by grafting the correct $1/r$ asymptotic tails onto the exchange-correlation potentials[18–20].

As to the computational aspect, the extant implementations of the TD-HF/DFT methods predominantly employ a linear combination of atomic orbitals (LCAO) approximation, most commonly using atom-centered Gaussian-type functions[21]. This allows for the second-quantization formulation of the linear response theory, in which the equation of interest, taking the form of a differential equation, is reduced to an algebraic eigenproblem with a finite matrix that is straightforward to implement. For the actual computations, the choice of basis sets used for the response calculations is rather problematic even when obtaining only a qualitative accuracy, since most standard basis sets are carefully designed to yield the best description of the ground-state wavefunction. Thus it is recommended to include polarized Gaussians with higher-order angular momentum and diffused Gaussians with small exponents. Moreover, the rapidly decaying tails of Gaussian functions give inefficient descriptions of diffuse shapes, which are often observed in response functions.

In the work of Refs.[1–3], we employed the multiresolution analysis (MRA) approach as an alternative numerical method for quantum chemical calculations. Our MRA approach is built upon Alpert's multiwavelet bases[4,22,23] for efficient, highly adaptive basis functions. All computations were performed to a user-defined, finite but mathematically guaranteed precision, so that the trade-off between precision and speed can be controlled systematically. We applied the MRA approach to the solution of the ground-state HF/KS equations for molecules[1,2] and the evaluation of their analytic derivatives[3]. Bischoff and Valeev presented the MRA approach to compute the HF wavefunction utilizing low-rank separated representation of the molecular orbitals, and to calculate the correlation energy using the pair function, e.g. the first-order Møller-Plesset (MP1) wavefunction, with analytic elimination of Coulombic singularities via explicit correlation[24–26]. Bischoff studied the regulation of the molecular potential in the MRA-based HF and MP2 calculations.[27,28] Frediani et al. reported a new implementation of the MRA solver with multiwavelet bases for DFT[29,30]. In a similar context, the use of the Daubechies wavelets in electronic structure calculations was investigated to develop the linear scaling DFT method[31–34].

In this study, we have applied the multiresolution approach to the TD-HF/DFT for the calculation of the energies of excited states. We present a reformulation to derive the one-particle response equation, which is fully expressed in the first-quantization form. No virtual orbitals are needed in the calculations of the response. The resultant working equation is efficiently solved using the integral equation solver for the Green's function. The density matrix operator plays a key role in projecting the equation onto the complementary space. The response functions and transition densities are represented adaptively with multiwavelet bases. The excitation energies meet the user-selected degree of accuracy. In Refs.[35,36], we illustrated response calculations for excited states and polarizabilties using our MRA code. In this paper, the details of the formulation to derive the response equation and the algorithm for computer implementation, which are a foundation of the work of Refs.[35,36], are presented along with detailed numerical assessment with CIS and TDDFT/TD calculations. In the next section, the multiresolution method is reviewed. The formulation of the TD-HF/DFT response equations is shown in Sec. III, and the computational algorithm and an implementation are presented in Secs. IV and V, respectively. The results are discussed in Sec. VI, and our conclusions are presented in Sec VII.

2 Background

Let us first give a brief overview of our MRA approach to quantum chemistry calculations. In the previous studies[1–3], we applied MRA to obtain a numerical solution of the HF/KS equations for polyatomic molecular systems. It uses the multiwavelet bases with disjoint supports, which are constructed from the first k Legendre or interpolating polynomials defined on disjoint intervals[4]. The details of the multiwavelet basis are given in our previous paper (Ref.[1]). The MRA with multiwavelet bases is capable of organizing functions and operators efficiently in terms of their proximity on a given scale and between different scales, and it provides a simple mechanism for truncation and adaptive refinement that can be used to maintain the desired accuracy. The adaptivity associated with the decomposition and refinement is key to representing globality and locality in the multiresolution hierarchy on an equal footing. Higher-order convergence can be achieved for solving partial differential and integral equation, and it can be maintained in the presence of boundary conditions or singularities. The vanishing moments property built into the multiwavelet bases assures a sparse representation of functions and operators.

In a previous paper[1], a numerical integral convolution operator with the Poisson and bound-state Helmholtz (BSH) kernels was developed in multiwavelet bases:

$$\mathscr{T} * f(r) = \int ds\, K(r-s)\, f(s), \qquad (1)$$

where $K(x)$ is the kernel of the integral operator $\mathscr{T}$. The nonstandard form (NS-form) of applying operators to func-

tions is an underlying algorithm that can exploit sparsity in the integration using multiwavelet bases[37–39]. In practice, the low-rank separation of the integral kernels was introduced in the three-dimensional integrator, and thus a prohibitively large computational overhead is avoided. This separation reduces the cost from $O(Mk^6)$ to $O(Mk^3)$, where M is the separation rank. The cost may be further reduced by applying the singular value decomposition to the one-dimensional separated integral operator.[1,40–42] In a previous study[1], we presented nearly optimal forms of the separated representations of the Poisson and BSH kernels, based on the quadrature rule of the integral forms of the kernels. The Poisson and BSH operators in three dimsnsions were implemented in the MRA integration solver.

The Poisson kernel $1/r$ arises in the evaluation of Coulomb operator $\hat{J}$ and the Hartree-Fock exchange operator $\hat{K}$:

$$\hat{J}[\rho] = \int dr' \frac{\rho(r',r')}{|r-r'|}, \tag{2}$$

and

$$\hat{K}[\rho] f(r) = \int dr' \frac{\rho(r,r') f(r')}{|r-r'|}. \tag{3}$$

The HF/KS equations are solved in the following integral equation form, which contains the BSH operator:

$$\begin{aligned} \psi_i &= -2\left(-\nabla^2 - 2\varepsilon_i\right)^{-1}\left(\hat{V}^0\psi_i\right), \\ &= -2\hat{G}(k) * \left(\hat{V}^0\psi_i\right), \end{aligned} \tag{4}$$

where $\{\psi_i\}$ and $\{\varepsilon_i\}$ are the canonical orbitals and orbital energies, respectively, $\hat{V}^0$ is the potential, $\hat{G}(k)$ is the BSH integral operator parameterized with $k = \sqrt{-2\varepsilon_i}$ (>0), and the integral kernel of $\hat{G}(k)$ is given by

$$G(r,r') = \frac{e^{-k|r-r'|}}{4\pi|r-r'|}. \tag{5}$$

In a previous paper[1], we presented a multiresolution solver for the one-particle eigenequation for the HF/KS self-consistent field (SCF) method.

3 Formulation of the TD-HF/DFT linear response method

The derivation of the linear response approach for the time-dependent Hartree-Fock and density functional theory (TD-HF/DFT) is now well established within the quantum chemistry literature[5]. It is normally based on the second-quantization formalism and yields an algebraic representation of the corresponding eigenequation; the basis representing the equation is taken from the one-particle SCF orbitals, and a finite number of virtual (unoccupied) orbitals serve as the complementary basis.

In our multiresolution approach, the basis is extremely large (nearly infinite), and the ground state calculations provide occupied orbitals alone. Therefore, it is necessary to reformulate the linear response so that the virtual orbitals, which may include continuum states, do not explicitly arise in the TD-HF/DFT calculations. It should also be noted that the TD-HF/DFT is a one-particle theory (i.e. three-dimensional) and thus it can be implemented within the extant framework of our multiresolution solver.

The formulation begins with the density matrix form of the TDHF equation derived by Dirac[6]:

$$\hat{F}\hat{\rho} - \hat{\rho}\hat{F} = i\frac{\partial}{\partial t}\hat{\rho}, \tag{6}$$

where $\hat{\rho}$ is the operator form of the Fock-Dirac density matrix, $\rho(r,r')$, which is represented by the occupied canonical orbitals $\{\phi_i(r)\}$ as:

$$\rho(r,r') = \sum_i^{occ} \phi_i(r)\phi_i^\dagger(r'), \tag{7}$$

where the occupied orbitals are orthonormal:

$$\int dr\, \phi_p^\dagger(r)\phi_q(r) = \delta_{pq}. \tag{8}$$

The density matrix operator (spectral operator) $\hat{\rho}$ is given in Dirac's bra-ket notation by

$$\hat{\rho} = \sum_i^{occ} |\phi_i\rangle\langle\phi_i|, \tag{9}$$

which serves as an operator that projects the function $f(r)$ onto the occupied orbital space:

$$\hat{\rho} f(r) = \sum_i^{occ} \phi_i(r) \int dr' \phi_i^\dagger(r') f(r'), \tag{10}$$

and is idempotent:

$$\hat{\rho} = \hat{\rho}\hat{\rho}. \tag{11}$$

The Fock operator $\hat{F}$ is defined with the one-electron core operator $\hat{h}$ and the electron-interaction operator $\hat{g}[\rho]$ by:

$$\hat{F} = \hat{h} + \hat{g}\left[\rho(r,r')\right]. \tag{12}$$

Applying an oscillatory perturbation allows us to partition the Fock operator and the density matrix into the time-independent and the time-dependent terms:

$$\hat{F} = \hat{F}^0 + \hat{F}', \tag{13}$$

$$\rho(r,r') = \rho^0(r,r') + \rho'(r,r'), \tag{14}$$

where the time-dependent terms $\hat{F}'$ and $\rho'(r,r')$ are regarded as perturbative. The anticommutation of the time-independent

Fock operator $\hat{F}^0$ and the density matrix $\rho^0(r,r')$ gives the density-matrix form of the unperturbed HF equation:

$$\hat{F}^0\hat{\rho}^0 - \hat{\rho}^0\hat{F}^0 = 0. \quad (15)$$

The perturbative time-dependent terms of the one-electron core operator and the density matrix induced in an oscillating applied field can be expressed as a single Fourier component:

$$\hat{h}' = \frac{1}{2}\left(Ae^{-i\omega t} + A^\dagger e^{i\omega t}\right), \quad (16)$$

$$\rho'(r,r') = \frac{1}{2}\left(d(r,r')e^{-i\omega t} + d^\dagger(r,r')e^{i\omega t}\right). \quad (17)$$

The perturbation of the electron-interaction term is written as:

$$\hat{g}'[\rho] = \hat{g}'\left[\rho^0+\rho'\right] \quad (18)$$

$$= \hat{g}'\left[\rho^0\right] + \frac{\partial\hat{g}}{\partial\rho}\left[\rho^0\right]*\rho', \quad (19)$$

where, for the Hartree-Fock potential, the last term in eq. (19) takes the form of an integral convolution. The time-independent and perturbative time-dependent terms of the Fock operator are thus given by:

$$\hat{F}^0 = \hat{h}^0 + \hat{g}\left[\rho^0\right], \quad (20)$$

$$\hat{F}' = \hat{h}' + \frac{\partial\hat{g}}{\partial\rho}\left[\rho^0\right]*\rho', \quad (21)$$

respectively. Inserting the above expressions into eq. (6) leads to the following equation for $\hat{d}$:

$$\left(\hat{F}^0\hat{d} - \hat{d}\hat{F}^0\right) + \left\{\left(\hat{A} + \frac{\partial\hat{g}}{\partial\rho}\left[\rho^0\right]*d\right)\hat{\rho}^0 - \hat{\rho}^0\left(\hat{A} + \frac{\partial\hat{g}}{\partial\rho}\left[\rho^0\right]*d\right)\right\} = \omega\hat{d}. \quad (22)$$

Applying $\left(1-\hat{\rho}^0\right)$ and $\hat{\rho}^0$ to eq. (22) from the left and right sides, respectively, gives

$$\left(1-\hat{\rho}^0\right)\hat{F}^0\left(1-\hat{\rho}^0\right)\hat{x} - \hat{x}\left(\hat{\rho}^0\right)\hat{F}^0\left(\hat{\rho}^0\right) + \left(1-\hat{\rho}^0\right)\left\{\hat{A} + \frac{\partial\hat{g}}{\partial\rho}\left[\rho^0\right]*(x+y)\right\}\left(\hat{\rho}^0\right) = \omega\hat{x}, \quad (23)$$

and applying $\hat{\rho}^0$ and $\left(1-\hat{\rho}^0\right)$ from the left and right sides, respectively, gives

$$\left(\hat{\rho}^0\right)\hat{F}^0\left(\hat{\rho}^0\right)\hat{y} - \hat{y}\left(1-\hat{\rho}^0\right)\hat{F}^0\left(1-\hat{\rho}^0\right) - \left(\hat{\rho}^0\right)\left\{\hat{A} + \frac{\partial\hat{g}}{\partial\rho}\left[\rho^0\right]*(x+y)\right\}\left(1-\hat{\rho}^0\right) = \omega\hat{y}, \quad (24)$$

where we introduce the substitutions $\hat{x}$ and $\hat{y}$, which correspond to:

$$\hat{x} = \left(1-\hat{\rho}^0\right)\hat{d}\left(\hat{\rho}^0\right), \ \hat{y} = \left(\hat{\rho}^0\right)\hat{d}\left(1-\hat{\rho}^0\right). \quad (25)$$

The following identity is evident:

$$\hat{d} = \left(\hat{\rho}^0 + 1 - \hat{\rho}^0\right)\hat{d}\left(\hat{\rho}^0 + 1 - \hat{\rho}^0\right) = \hat{x} + \hat{y}. \quad (26)$$

The transition density matrix operators $\hat{x}$ and $\hat{y}$ account for the occupied-unoccupied and unoccupied-occupied transitions. The transition matrices $x(r,r')$ and $y(r,r')$ can thus be expanded into a linear combination of the occupied orbitals:

$$x(r,r') = \sum_i^{occ} x_i(r)\,\phi_i^\dagger(r'), \quad (27)$$

$$y(r,r') = \sum_i^{occ} \phi_i(r)\,y_i^\dagger(r'), \quad (28)$$

where the functions $x_i(r)$ and $y_i(r)$ are the response functions. In the conventional matrix-based second-quantization formulation, the response functions $x_i(r)$ and $y_i(r)$ are expressed using the virtual orbitals $\{\psi_a\}$ as the basis and with the tran-

sition coefficients (or CIS coefficients) $\{x_{ai}, y_{ai}\}$:

$$x_i(r) = \sum_a^{vir} \phi_a(r) x_{ai}, \quad (29)$$

$$y_i(r) = \sum_a^{vir} \phi_a(r) y_{ai}. \quad (30)$$

In contrast, the multiresolution method yields fully numerical representations for the response functions $x_i(r)$ and $y_i(r)$ in multiwavelet bases in an efficient, adaptive fashion.

The operator terms $(\hat{\rho}^0)\hat{d}(\hat{\rho}^0)$ and $(1-\hat{\rho}^0)\hat{d}(1-\hat{\rho}^0)$ correspond to the occupied-occupied and unoccupied-unoccupied elements, which are both zero. We assume that the electronic transitions occur with an infinitesimal perturbation:

$$(1-\hat{\rho}^0)\hat{A}(\hat{\rho}^0) = (\hat{\rho}^0)\hat{A}(1-\hat{\rho}^0) = 0. \quad (31)$$

According to the relations of eqs. (8), (27), (28), and (31), and with the orbital energy given by $\varepsilon_p^0 = \int dr\, \phi_p^\dagger(r)\hat{F}^0\phi_p(r)$, we arrived at the following coupled response eigenequations for x_p, y_p, and ω:

$$(1-\hat{\rho}^0)\left[(\hat{F}^0-\varepsilon_p^0)x_p(r) + \left\{\frac{\partial\hat{g}}{\partial\rho}[\rho^0] * \left(\sum_i^{occ} x_i(r)\phi_i^\dagger(r') + \sum_i^{occ}\phi_i(r)y_i^\dagger(r')\right)\right\}\phi_p(r)\right] = \omega x_p(r), \quad (32)$$

$$(1-\hat{\rho}^0)^\dagger\left[(\hat{F}^0-\varepsilon_p^0)^\dagger y_p(r) + \left\{\frac{\partial\hat{g}}{\partial\rho}[\rho^0] * \left(\sum_i^{occ} x_i(r)\phi_i^\dagger(r') + \sum_i^{occ}\phi_i(r)y_i^\dagger(r')\right)\right\}^\dagger\phi_p(r)\right] = -\omega y_p(r), \quad (33)$$

where we have multiplied eqs. (23) and (24) by the occupied orbitals from the right and left sides, respectively.

The Tamm-Dancoff approximation, which neglects the terms that involve $y_p(r)$, leads to the following simpler equation:

$$(1-\hat{\rho}^0)\left[(\hat{F}^0-\varepsilon_p^0)x_p(r) + \left\{\frac{\partial\hat{g}}{\partial\rho}[\rho^0] * \left(\sum_i^{occ} x_i(r)\phi_i^\dagger(r')\right)\right\}\phi_p(r)\right] = \omega x_p(r). \quad (34)$$

4 Numerical algorithm and implementation

This section describes a computational algorithm that is implemented in the multiresolution solver for solving the response equation, eq. (34). To create an implementable form of eq. (34), we begin by transforming it to the following intermediate:

$$\left[\hat{F}^0 - (\varepsilon_p^0+\omega)\right]x_p(r) = -(1-\hat{\rho}^0)\Gamma_p(r), \quad (35)$$

where we used the relations $\hat{\rho}^0 x_p(r) = 0$ and $\hat{F}^0\hat{\rho}^0 = \hat{\rho}^0\hat{F}^0$. For convenience, we will substitute $\Gamma_p(r)$ for the electron interaction term:

$$\Gamma_p(r) = \left\{\frac{\partial\hat{g}}{\partial\rho}[\rho^0] * \left(\sum_i^{occ} x_i(r)\phi_i^\dagger(r')\right)\right\}\phi_p(r). \quad (36)$$

Substituting the Fock operator $\hat{F}^0$ with $-\nabla^2/2 + \hat{V}^0$, we will obtain the following integral equation:

$$\begin{aligned}\tilde{x}_p(r) &= -2\left[-\nabla^2 - 2(\varepsilon_p^0+\omega)\right]^{-1}\left[\hat{V}^0 x_p(r) + (1-\hat{\rho}^0)\Gamma_p(r)\right], \\ &= -2\hat{G}(k) * \left[\hat{V}^0 x_p(r) + (1-\hat{\rho}^0)\Gamma_p(r)\right], \end{aligned} \quad (37)$$

where

$$k = \sqrt{-2(\varepsilon_p^0+\omega)}. \quad (38)$$

The integral convolution operator $\hat{G}(k)$ in eq. (37) is the same operator as that in eq. (4), which we employed in the multiresolution solver for the HF/KS-SCF method (Sec. 2). In this

sense, the algorithms for the HF/KS-SCF method and the linear response method may be analogous.

Our implementation of the linear response theory updates response functions by iterating the application of the convolution integral operator, eq. (37). Because the free-space boundary conditions are assumed, the integral operator is limited to a kernel with a non-imaginary k, i.e., k is zero (for the Poisson kernel) or a positive real number (for the BSH kernel). If eq. (38) is imaginary, i.e., $\varepsilon_p^0 + \omega > 0$, we can employ the following equation with a shifting constant $\Delta(<0)$, instead of eq. (37):

$$\tilde{x}_p(r) = -2\hat{G}(k') * \left[\hat{V}^0 x_p(r) + \left(1-\hat{\rho}^0\right)\Gamma_p(r) + \Delta x_p(r)\right], \tag{39}$$

where $k' = \sqrt{-2\left(\varepsilon_p^0 + \omega + \Delta\right)}$ is zero or a small positive real number. If eq. (38) does not converge to a real number, the solution is unbound. The unbound excitation state corresponds to a continuum scattering state, and its excitation energy is above the ionization potential.

Next, we show the specific expressions of the electron interaction (eq. (36)) for the Coulomb, HF exchange, and local spin-density approximation (LSDA) exchange-correlation potentials. The electron-interaction term for the Coulomb operator $\hat{g}[\rho] = \hat{J}[\rho]$, eq. (2), is given by

$$\begin{aligned}\mathscr{J}_p(r) &= \left\{\frac{\partial \hat{J}}{\partial \rho}\left[\rho^0\right] * \left(\sum_i^{occ} x_i(r)\,\phi_i^\dagger(r')\right)\right\}\phi_p(r), \\ &= \left(\sum_i^{occ}\int dr' \frac{x_i(r')\,\phi_i^\dagger(r')}{|r-r'|}\right)\phi_p(r), \end{aligned} \tag{40}$$

and for the HF exchange operator $\hat{g}[\rho] = \hat{K}[\rho]$, eq. (3), by

$$\begin{aligned}\mathscr{K}_p(r) &= \left\{\frac{\partial \hat{K}}{\partial \rho}\left[\rho^0\right] * \left(\sum_i^{occ} x_i(r)\,\phi_i^\dagger(r')\right)\right\}\phi_p(r), \\ &= \sum_i^{occ} x_i(r)\int dr' \frac{\phi_i^\dagger(r')\,\phi_p(r')}{|r-r'|}. \end{aligned} \tag{41}$$

The LSDA exchange-correlation potential is given by

$$\hat{g}[\rho] = V_{xc}[\rho] = \frac{\delta E_{xc}[\rho]}{\delta \rho}, \tag{42}$$

and the electron-interaction term for the TDDFT calculations is thus given by

$$\mathscr{W}_p(r) = \left\{\frac{\partial^2 E_{xc}}{\partial \rho^2}\left[\rho^0\right]\left(\sum_i^{occ} x_i(r)\,\phi_i^\dagger(r)\right)\right\}\phi_p(r), \tag{43}$$

where E_{xc} is the exchange-correlation functional.

The above Coulomb and HF exchange operators are evaluated using the multiresolution integral solver for the integral convolution operator with a Poisson kernel. When calculating the HF exchange term, eq (41), the integrals $\int dr' \phi_i^\dagger(r')\,\phi_p(r')/|r-r'|$ are precalculated and stored, so that the integrals do not need to be recalculated at every iteration; however, the memory required for this is on the order of $N_{occ} \times (N_{occ}+1)/2$.

The TDDFT calculations require the numerical representation of the second derivative of the exchange-correlation functional with respect to the density, $\partial^2 E_{xc}/\partial \rho^2\left[\rho^0\right]$. Since the functional is dependent on only the density function that is made from occupied orbitals, the evaluation of the second derivative of the exchange-correction functional is only performed once, prior to the iterations. The computations include a one-centered (local) numerical operation on the density function, and so the computational cost is $O(N)$.

For our prototype implementation of the TD-HF/DFT linear response method in the experimental version of the multiresolution solver MADNESS, we reused most of the HF/KS-SCF computer programming code developed a previous study[1]. The Krylov-subspace accelerated inexact Newton (KAIN) method[43] is used to accelerate convergence. The second derivative of the exchange-correlation functional is computed using a subroutine library implemented in NWCHEM[44]. The programming structure is summarized as follows:

1. Obtain the occupied orbitals $\{\phi_p\}$, their orbital energies $\{\varepsilon_p^0\}$, and the density function ρ^0 from a HF/KS-SCF calculation in the MRA approach.

2. Compute a numerical representation of the second derivative of the exchange-correlation functional, $\partial^2 E_{xc}/\partial \rho^2\left[\rho^0\right]$.

3. Prepare the initial response functions $\{x_p^{(k)}\}$ of the required states $k = 1,\ldots,N^{states}$. They can be generated from a preliminary Gaussian calculation according to the relation given in eq. (29).

4. Compute the transition density function $x(r)$, eq. (27), which is a sum of the products of the occupied orbitals and the response functions.

5. Obtain $\left\{\Gamma_p^{(k)}\right\}$ in eq. (36) from the computation of $\left\{\mathscr{J}_p^{(k)}\right\}$, $\left\{\mathscr{K}_p^{(k)}\right\}$, and $\left\{\mathscr{W}_p^{(k)}\right\}$ in eqs. (40), (41), and (43), respectively.

6. Compute $\hat{V}^0 x_p^{(k)}$. Note that, except for the HF exchange potential, $\hat{V}_0$ is a local potential, which is thus already obtained in the ground-state calculation.

7. [*in the first iteration or for deflation*]
Obtain the initial eigenvalues $\omega^{(k)}$ from the following matrix diagonalization,

$$\mathbf{Ax} = \mathbf{Sx}\omega, \tag{44}$$

where

$$A_{ij} = \sum_p \int dr x_p^{(i)} \left(1-\hat{\rho}^0\right) \left[\left(\hat{F}^0 - \varepsilon_p^0\right) x_p^{(j)}(r) + \Gamma_p^{(j)}(r)\,\phi_p(r)\right], \tag{45}$$

$$S_{ij} = \sum_p \int dr x_p^{(i)}(r) x_p^{(j)}(r)\,. \tag{46}$$

The differential operator needs to be evaluated in the Fock operator. The matrix elements A_{ij} and S_{ij} that are of integral form can be computed as inner products.

8. Compute the projection: $\left(1-\hat{\rho}^0\right)\Gamma_p^{(k)}$.

9. Apply the BSH integral operators to the integral equations, eq. (37).

10. The trail eigenvalues $\omega^{(k)}$ are corrected according to the following preconditioned correction[1]:

$$\delta\omega^{(k)} = -\frac{\sum_p \left\langle \hat{V}^0 x_p^{(k)}(r) + \left(1-\hat{\rho}^0\right)\Gamma_p^{(k)}(r) \,\middle|\, x_p^{(k)} - \tilde{x}_p^{(k)} \right\rangle}{\sum_p \|\tilde{x}_p^{(k)}\|^2}. \tag{47}$$

11. Apply Gram-Schmidt orthonormalization to the response functions such that $\sum_p \langle x_p^{(k)} | x_p^{(k')} \rangle = \delta_{kk'}$.

12. Repeat from step 4 through step 11 until the residual is smaller than a predetermined threshold value.

5 Results

5.1 CIS calculation for hydrogen molecule

The initial test of the multiresolution solver for the linear response method was performed upon an H_2 molecule. The bond length and the box size are set to 1.4 bohr and 200 bohr, respectively.

Table 1 lists the orbital energies of the occupied orbitals for the 7-, 9-, and 11-th multiwavelet bases, noted by $k = 7$, 9, and 11, respectively, when the residual of the MO equation is less than $3\times10^4 (k=7)$, $3\times10^5 (k=7)$, $3\times10^6 (k=9)$, and $3\times10^7 (k=11)$. The table includes the orbital energies computed with four kinds of Gaussian-type functions: cc-pVTZ, augmented cc-pVTZ, doubly augmented cc-pVTZ, and doubly augmented cc-pVQZ[45,46]. The Gaussian calculations were performed using NWCHEM[44]. The error of the computed orbital energy is estimated as the deviation from the most accurate result determined with $k = 11$. As seen in the study presented in Ref.[1], the errors in the multiresolution calculations are in proportion to the residuals. The accuracy of the orbital energy when using d-aug-cc-pVQZ is comparable to that with $k = 7$ and the residual 3×10^{-4}.

Table 2 shows the CIS excitation energies for 16 low-lying singlet and triplet excited states. The CIS calculations met the convergence criteria when the residual of the equation with the response functions was less than the residual in the corresponding occupied orbital. Figure 1 shows a plot of the absolute errors, which are defined as the difference between the calculated energy and that for k=11. Overall, the multiresolution calculations yielded sufficient and consistent accuracy at the lowest excitation level through the higher excitations, including Rydberg states. The accuracy of the excitation energies attained in the multiresolution calculations is in proportion to the residuals of the response function. In the Gaussian calculations, the accuracy of the excitation energies was inconsistent over the different states. The addition of extra diffuse functions improved the description of the higher excitations, and there was poorer convergence with the lower quality basis sets.

The response functions and the MOs computed with k=7 are plotted in Figure 2. In the graph, we can see that the asymptotic behavior is exponential, and thus it is correctly described by the multiresolution approach. We observe that the most broadly diffused response function reaches a value of more than 10^{-3} at a distance of 50 bohr from the molecular center. The exponents used to fit the exponential functions to the asymptotic tails are listed in Table 3. Using these exponents, the orbital energy and the excitation energies can be estimated to within an error of 0.5 eV by using the analytic asymptotic form $\exp\left(-\sqrt{-2\varepsilon}\,x\right)$, where ε is the energy.

The response functions and the MOs obtained in the multiresolution (k=7) and Gaussian (d-aug-cc-pVTZ) calculations are shown in Figure 3. The function curves of the two calculations overlap near the valence region, except for the $^1\Pi_g$ state. However, we note that the asymptotic tails of the Gaussian results are away from the correct exponential form. This seems to result from the variational procedure with the Gaussian basis which does not precondition the eigenfunctions to have the proper asymptotic form, and thus the energies of the excited states are not consistently accurate. However, the energetic contributions from these errors are in fact small because most of the excitation energy is recovered through the description of the valence. As for the $^1\Pi_g$ state, the Gaussian calculation cannot reproduce the correct shape in the valence region.

5.2 TD-HF/DFT calculation with TD approximation for a beryllium atom

Next, the TD-HF/DFT calculations with the TD approximation were performed for a beryllium atom. Table 4 shows the highest occupied orbital and the total energies for the HF/KS-SCF calculations. The excitation energies are shown in Table 5. The present calculations were performed using the 7-th multiwavelet bases, the residuals of the calculated MOs and response functions were less than 1×10^{-4}, and a core orbital was frozen. Both tables include the Gaussian results reported by Hirata et al.[18].

The CIS results obtained by the multiresolution and Gaussian methods are in close accord. In the DFT calculations, the local spin-density approximation (LSDA) exchange-correlation functional was employed with and without the asymptotic correction. In Ref.[18], Hirata et al. proposed and used the asymptotically corrected LSDA potential (LSDA/AC), where the correct -1/r asymptotic form was enforced on the exchange-correlation potential by using the Slater potential[47] in the asymptotic region. The Slater potential[47] is given by

$$V^S(r) = -\sum_{i,j}^{occ} \frac{\phi_i(r)\,\phi_j(r)}{\rho(r)} \int dr' \frac{\phi_i(r')\,\phi_j(r')}{|r-r'|}. \qquad (48)$$

The potential in the vicinity of the nuclei is shifted by a constant, which is non-empirically determined by insisting that the shifted potential is that of the highest occupied molecular orbital (HOMO)[48]. The shifted potential and the Slater term are grafted to each other where they cross, except when the crossing occurs within the Bragg-Slater radius of any of the constituent nuclei.

Inspired by Hirata's insight, we employed the following simple, asymptotically corrected LSDA potential (AC-LSDA) in the multiresolution TDDFT/TD calculation:

$$V^{AC-LSDA}(r) = \begin{cases} V^{LSDA}(r) + \varepsilon_h^{HF} - \varepsilon_h^{LSDA}, & (\rho(r) \geq \rho_A), \\ \min\left(V^{LSDA}(r), V^S(r)\right), & \left(\rho_A > \rho(r) \geq 10^{-11}\right), \\ 0, & \left(10^{-11} > \rho(r) \geq 0\right), \end{cases} \qquad (49)$$

where the shifted constants ε_h^{HF} and ε_h^{LSDA} are the highest occupied orbital energies for the HF and LSDA calculations, respectively. An empirical parameter ρ_A is used to determine the point at which the potentials are grafted and thus discontinuous. In eq.(49), the Slater potential is used in the region of low electron density, and the shifted LSDA potential is used in the region of high electron density. Figure 4 shows a graph of the AC-LSDA potential for the Be calculation with the empirical parameter $\rho_A = 10^{-2}$. The $-1/r$ asymptotic behavior is observed in the AC-LSDA potential in the region between $r = 5.0$ bohr and $r = 15.0$ bohr. The discontinuity at $r > 15.0$ bohr arises due to the numerical instability of the denominator $\rho(r)$ in eq.(48). The figure also shows that the standard (non-AC) LSDA potential decays exponentially.

As shown in Tables 4 and 5, the AC-LSDA potential appears to improve the highest occupied orbital and excitation energies. The highest occupied orbital energy with the AC-LSDA potential is close to the HF orbital energy. Hirata's asymptotic correction does not affect the total energy, whereas the present AC-LSDA potential underestimated the total energy by 2.4 millihartree. In the standard (non-AC) LSDA excitation calculation, three lower-lying states are bound, and the other nine states are unbound. Five out of the nine unbound states did not meet the convergence criteria. On the other hand, the asymptotic correction to the LSDA potential yields eight bound states and four unbound states, all of which converged. The excitation energies determined with the AC-LSDA potential are closer to the experimental values than are those calculated with the LSDA/AC potential.

Figures 5, 6, and 7 show plots of the highest occupied orbital, and the bound and the unbound response functions, respectively for singlet states in TD-HF/DFT calculations. In the HF and CIS calculations, all the response functions are bound, and their asymptotic behaviors are exponential (Figure 5). Similarly, Figures 6 and 7 illustrate that the asymptotic exponential shapes of the bound-state functions obtained with the LSDA and AC-LSDA potentials. In these figures, the unbound response functions that do not decay are shown to vanish inside the box; at the side of the box, the boundary condition is artificially enforced by a masking function to be equal to the unbound response[1]. The physical model behind the LSDA is that the density can be treated locally as a uniform electron gas, or equivalently, that the density is a slowly varying function. The unbound response functions capture the aspect of the physical model in which the excitation is a continuum. Considering this, the multiresolution solver yielded a qualitatively correct description of the given physical model. Table 6 shows the estimated highest occupied orbital and singlet excitation energies obtained by fitting the asymptotic tails to exponential functions. This estimation is in good agreement with the actual value to within an error of 0.50 eV.

5.3 TD-HF/DFT excitation energies with TD approximation for N_2, H_2O, and C_2H_4 molecules

We used the multiresolution TD-HF/DFT methods to calculate the excitations for three small molecules, N_2, H_2O, and C_2H_4. Tables 7, 9, and 11 list the highest occupied orbital energies of the molecules with the equilibrium geometries. Tables 8, 10, and 12 summarize the vertical excitation energies and the experimental data[49–51], the Gaussian results reported by Hirata et al. for N_2 and H_2O[18], and those calculated with d-aug-cc-pVTZ Gaussian basis sets for C_2H_4. The multiresolution

calculations were performed with the 7-th multiwavelet bases, with the residual of the equation expressed in MOs and the response functions restricted to be less than 1×10^{-4}, and the core orbitals frozen. For the HF and CIS results, the mean absolute differences between the excitation energies of the multiresolution calculations and the Gaussian calculations were 0.03 eV, 0.06 eV, and 0.04 eV for N_2, H_2O, and C_2H_4, respectively, and the maximum differences were 0.09 eV ($^3\Pi_u$), 0.11 eV ($^3B_1$), and 0.25 eV ($^1B_{3u}$), respectively. In the AC-LSDA calculations, the empirical parameter was chosen to be $\rho_A = 10^{-2}$, 10^{-3}, and 10^{-3} for N_2, H_2O, and C_2H_4, respectively. The asymptotic correlation yielded no unbound state throughout the calculations. The AC-LSDA calculations for the $^1\Pi_u$ state for N_2 and the $^3A_1$ state for H_2O did not converge. The lack of convergence seems to be caused by the unstable numerical representations of the second derivative of the exchange-correlation functional. The lower excitation energies obtained with the AC-LSDA potential are in good agreement with those obtained with Hirata's LSDA/AC potentials, as well as with the experimental values. On the other hand, the AC-LSDA potential does not satisfactorily reproduce the higher excitation energies found in the experiment.

6 Conclusions

We have presented a multiresolution approach to calculating the fully numerical linear response for excited states on the basis of the TD-HF/DFT with the Tamm-Dancoff approximation. The calculations are performed by iteratively solving the integral equation, using the BSH kernel for the Green's function. The basis errors are adaptively refined by the MRA, and thus, when calculating the energies of excited states at a variety of length scales, from short-range valence excitations to long-range Rydberg-type ones, we can efficiently and consistently attain an arbitrary numerical accuracy. Our method is capable of efficiently delivering the basis function limits of the TD-HF/DFT excitation energies.

We reformulated the linear response theory from the TD-HF/DFT equation into the first-quantization form. The resultant equation takes a general form that does not explicitly involve virtual orbitals, and thus the equation can be implemented in a multiresolution solver where the complementary basis for the virtual orbital space is nearly infinite. We showed that the HF/KS-SCF algorithm is analogous to the TD-HF/DFT linear response method in that they both solve an integral equation by using the BSH integral convolution operator.

We presented the illustrative TD-HF/DFT calculations for H_2, Be, N_2, H_2O, and C_2H_4. The CIS calculation for H_2 revealed that the numerical errors of the excitation energies in the multiresolution approach converge in proportion to the residuals of the equation based on the response functions. The accuracy is consistent over the various states. The asymptotic tails of the response functions were clearly shown to decay exponentially. These results indicate that the integral operators for excited states can be adaptively represented in our multiresolution scheme with a controllable accuracy. In the TDDFT/TD calculations for Be, N_2, H_2O, and C_2H_4, we used the Slater potential as a simple asymptotic correction to the LSDA potential. Due to the $-1/r$ asymptotic behavior in the modified exchange-correlation potential, we obtained the correct bound states.

Acknowledgment

We are grateful to Dr. So Hirata for helpful guidance and valuable discussions about the linear response theory.

RJH, TY, and GF were funded by the Scientific Discovery through Advanced Computing (SciDAC) program of the U.S. Department of Energy, the division of Basic Energy Science, Office of Science, under contract DE-AC05-00OR22725 with Oak Ridge National Laboratory. GF was partially supported by the Office of Advanced Scientific Computing Research, Program in Mathematics, Information, and Computer Science through the Scientific Application Prototype Program of SciDAC.

The work of GB was supported in part by a University of Virginia subcontract under Grant MDA972-00-1-0016 and NSF/ITR Grants ACI-0082982 and DMS-0219326.

This research was performed in part using the resources of the National Energy Scientific Computing Center, which is supported by the Office of Energy Research of the U.S. Department of Energy under contract DE-AC03-76SF0098, and the Center for Computational Sciences at Oak Ridge National Laboratory under contract DE-AC05-00OR22725.

References

1 R. J. Harrison, G. I. Fann, T. Yanai, Z. Gan and G. Beylkin, *J. Chem. Phys.*, 2004, **121**, 11587.
2 T. Yanai, G. I. Fann, Z. Gan, R. J. Harrison and G. Beylkin, *J. Chem. Phys.*, 2004, **121**, 6680.
3 T. Yanai, G. I. Fann, Z. Gan, R. J. Harrison and G. Beylkin, *J. Chem. Phys.*, 2004, **121**, 2866.
4 B. Alpert, G. Beylkin, D. Gines and L. Vozovoi, *J. Comp. Phys.*, 2002, **182**, 149.
5 R. McWeeny, *Methods of Molecular Quantum Mechanics, 2nd ed.*, Academic Press, London, 1992.
6 P. A. M. Dirac, *Proc. Camb. Phil. Soc.*, 1931, **27**, 240.
7 J. Frenkel, *Wave Mechanics, Advanced General Theory, Clarendon*, 1934.
8 D. J. Thouless, *The Quantum Mechanics of Many-Body Systems*, 1961.
9 E. Runge and E. K. U. Gross, *Phys. Rev. Lett.*, 1984, **52**, 997.
10 E. K. U. Gross and W. Kohn, *Adv. Quantum. Chem.*, 1990, **21**, 255.
11 E. Gross, C. Ullrich and U. Gossmann, *Density Functional Theory*, Springer, 1995, pp. 149–171.
12 M. Petersilka, U. J. Gossmann and E. K. U. Gross, *Phys. Rev. Lett.*, 1996, **76**, 1212.
13 M. E. Casida, *Recent advances in density functional methods, Part I*, World Scientific: Singapore, 1995, vol. 1, p. 155.
14 R. Bauernschmitt and R. Ahlrichs, *Chem. Phys. Lett.*, 1996, **256**, 454.
15 S. M. Colwell, N. C. Handy and A. M. Lee, *Phys. Rev. A*, 1996, **53**, 1316.
16 S. Hirata and M. Head-Gordon, *Chem. Phys. Lett.*, 1999, **302**, 375.
17 S. Hirata and M. Head-Gordon, *Chem. Phys. Lett.*, 1999, **314**, 291.
18 S. Hirata, S. Ivanov, I. Grabowski and R. J. Bartlett, *J. Chem. Phys.*, 2002, **116**, 6468.
19 M. E. Casida, C. Jamorski, K. C. Casida and D. R. Salahub, *J. Chem. Phys.*, 1998, **108**, 4439.
20 D. J. Tozer and N. C. Handy, *J. Chem. Phys.*, 1998, **109**, 10180.
21 S. F. Boys, *Proc. Roy. Soc. London*, 1950, **A200**, 542.
22 B. K. Alpert, *SIAM J. Math. Anal.*, 1993, **24**, 246.
23 B. Alpert, G. Beylkin, R. Coifman and V. Rokhlin, *SIAM J. Sci. Comput.*, 1993, **14**, 159.
24 F. A. Bischoff and E. F. Valeev, *J. Chem. Phys.*, 2011, **134**, 104104.
25 F. A. Bischoff, R. J. Harrison and E. F. Valeev, *J. Chem. Phys.*, 2012, **137**, 104103.
26 F. A. Bischoff and E. F. Valeev, *J. Chem. Phys.*, 2013, **139**, 114106.
27 F. A. Bischoff, *J. Chem. Phys.*, 2014, **141**, 184105.
28 F. A. Bischoff, *J. Chem. Phys.*, 2014, **141**, 184106.
29 T. F. . K. R. Luca Frediani, Eirik Fossgaard, *Mol. Phys.*, 2013, **111**, 1143.
30 S. R. Jensen, J. Jusélius, A. Durdek, T. Flå, P. Wind and L. Frediani, *Int. J. Model. Simul. Sci. Comput.*, 2014, **05**, 1441003.
31 T. A. Arias, *Rev. Mod. Phys.*, 1999, **71**, 267.
32 L. Genovese, T. Deutsch, A. Neelov, S. Goedecker and G. Beylkin, *J. Chem. Phys.*, 2006, **125**, 074105.
33 L. Genovese, A. Neelov, S. Goedecker, T. Deutsch, S. A. Ghasemi, A. Willand, D. Caliste, O. Zilberberg, M. Rayson, A. Bergman and R. Schneider, *J. Chem. Phys.*, 2008, **129**, 014109.
34 S. Mohr, L. E. Ratcliff, P. Boulanger, L. Genovese, D. Caliste, T. Deutsch and S. Goedecker, *J. Chem. Phys.*, 2014, **140**, 204110.
35 T. Yanai, R. J. Harrison and N. C. Handy, *Mol. Phys.*, 2005, **103**, 413.
36 H. Sekino, Y. Maeda, T. Yanai and R. J. Harrison, *J. Chem. Phys.*, 2008, **129**, 034111.
37 G. Beylkin, R. R. Coifman and V. Rokhlin, *Comm. Pure and Appl. Math.*, 1991, **44**, 141.
38 D. Gines, G. Beylkin and J. Dunn, *Appl. Comput. Harmon. Anal*, 1998, **5**, 156.
39 G. Beylkin, V. Cheruvu and F. Perez, *Appl. Comput. Harmon. Anal.*, 2008, **24**, 354.
40 R. J. Harrison, G. I. Fann, T. Yanai and G. Beylkin, *Computational Science ICCS 2003*, Springer, 2003, p. 103.
41 G. Beylkin and M. Mohlenkamp, *Proc. Natl. Acad. Sci. USA*, 2002, **99**, 10246.
42 G. Beylkin and M. Mohlenkamp, *SIAM J. Sci. Comput.*, 2005, **26**, 2133.
43 R. J. Harrison, *J. Comp. Chem.*, 2004, **25**, 328.
44 *"NWChem, A Computational Chemistry Package for Parallel Computers, Version 4.1,"* R. J. Harrison, J. A. Nichols, T. P. Straatsma, M. Dupuis, E. J. Bylaska, G. I. Fann, T. L. Windus, E. Apra, W. de Jong, S. Hirata, M. T. Hackler, J. Anchell, D. Bernholdt, P. Borowski, T. Clark, D. Clerc, H. Dachsel, M. Deegan, K. Dyall, D. Elwood, H. Fruchtl, E. Glendening, M. Gutowski, K. Hirao, A. Hess, J. Jaffe, B. Johnson, J. Ju, R. Kendall, R. Kobayashi, R. Kutteh, Z. Lin, R. Littlefield, X. Long, B. Meng, T. Nakajima, J. Nieplocha, S. Niu, M. Rosing, G. Sandrone, M. Stave, H. Taylor, G. Thomas, J. van Lenthe, K. Wolinski, A. Wong, and Z. Zhang, 2002, Pacific Northwest National Laboratory, Richland, Washington 99352-0999, USA.
45 T. H. Dunning, *J. Chem. Phys.*, 1989, **90**, 1007.
46 R. A. Kendall, T. H. Dunning and R. J. Harrison, *J. Chem. Phys.*, 1992, **96**, 6796.
47 J. C. Slater, *Phys. Rev.*, 1951, **81**, 385.
48 J. B. Krieger, Y. Li and G. J. Iafrate, *Phys. Rev. A*, 1992, **45**, 101.
49 S. B. Ben-Shlomo and U. Kaldor, *J. Chem. Phys.*, 1990, **92**, 3680.
50 R. J. Buenker and S. D. Peyerimhoff, *Chem. Phys. Lett.*, 1974, **29**, 253.
51 L. Serrano-Andres, M. Merchan, I. Nebot-Gil, R. Lindh and B. O. Roos, *J. Chem. Phys.*, 1993, **98**, 3151.
52 *NIST Chemistry Web Book, NIST Standard Reference Database Number 69*, edited by P. J. Linstrom and W. G. Mallard (http://webbook.nis.gov) (National Institute of Standards and Technology, Gaithersburg, MD, 2001.).
53 R. L. Graham, D. L. Yeager, J. Olsen, P. Jølgensen, R. Harrison, S. Zarrabian and R. Bartlett, *J. Chem. Phys.*, 1986, **85**, 6544.

Table 1 The occupied orbital energies (ε_h) and their absolute errors (in hartree) of H_2 (1.4 bohr) for the Hartree-Fock calculation.

basis	ε_h	error
cc-pVTZ	-0.594 427 8	2.3×10^{-4}
aug-cc-pVTZ	-0.594 401 3	2.6×10^{-4}
d-aug-cc-pVTZ	-0.594 391 2	2.7×10^{-4}
d-aug-cc-pVQZ	-0.594 613 2	4.5×10^{-5}
k=7, resi.$< 3 \times 10^{-4}$	-0.594 640 678	1.7×10^{-5}
k=7, resi.$< 3 \times 10^{-5}$	-0.594 658 893	1.0×10^{-6}
k=9, resi.$< 3 \times 10^{-6}$	-0.594 658 059	1.6×10^{-7}
k=11, resi.$< 3 \times 10^{-7}$	-0.594 657 898	—

Table 2 CIS excitation energies (in eV) of H_2 (1.4 bohr).

Singlet	$1^1\Sigma_u$	$1^1\Sigma_g$	$^1\Pi_u$	$2^1\Sigma_u$	$2^1\Sigma_g$	$^1\Pi_g$
NWCHEM						
cc-pVTZ	13.650 165 9	17.596 907 9	25.314 912 3	25.505 121 3	35.581 912 4	35.748 789 2
aug-cc-pVTZ	12.737 747 2	13.049 851 9	14.509 656 8	15.686 788 7	17.794 154 2	17.938 899 6
d-aug-cc-pVTZ	12.732 600 5	13.003 349 8	13.104 064 4	14.652 878 3	14.753 335 3	14.876 899 2
d-aug-cc-pVQZ	12.735 882 3	13.005 346 5	13.103 891 7	14.651 825 1	14.753 877 2	14.827 928 5
MADNESS						
k=7, resi.$< 3 \times 10^{-4}$	12.735 100 6	13.002 657 8	13.097 734 9	14.639 356 4	14.737 035 4	14.665 801 7
k=7, resi.$< 3 \times 10^{-5}$	12.735 615 2	13.003 186 5	13.098 184 2	14.639 887 3	14.737 841 4	14.666 288 4
k=9, resi.$< 3 \times 10^{-6}$	12.735 626 8	13.003 222 0	13.098 152 7	14.639 874 2	14.737 851 6	14.666 268 2
k=11, resi.$< 3 \times 10^{-7}$	12.735 622 3	13.003 217 6	13.098 147 1	14.639 869 1	14.737 849 9	14.666 263 2
Triplet	$1^3\Sigma_u$	$1^3\Sigma_g$	$^3\Pi_u$	$2^3\Sigma_u$	$2^3\Sigma_g$	$^3\Pi_g$
NWCHEM						
cc-pVTZ	10.043 032 3	14.260 537 1	20.543 507 6	21.203 595 0	33.154 165 5	34.087 700 8
aug-cc-pVTZ	9.978 537 7	12.031 541 4	12.883 666 5	14.412 837 4	17.032 021 4	17.737 789 1
d-aug-cc-pVTZ	9.976 522 6	12.029 900 4	12.310 131 7	14.189 012 5	14.497 603 1	14.855 307 8
d-aug-cc-pVQZ	9.978 642 5	12.033 841 4	12.311 513 4	14.178 500 2	14.503 321 6	14.808 992 0
MADNESS						
k=7, resi.$< 3 \times 10^{-4}$	9.977 728 3	12.029 871 7	12.308 381 0	14.157 228 0	14.499 081 9	14.654 812 5
k=7, resi.$< 3 \times 10^{-5}$	9.978 134 1	12.030 259 1	12.308 505 0	14.157 799 3	14.499 461 4	14.655 313 1
k=9, resi.$< 3 \times 10^{-6}$	9.978 116 6	12.030 233 9	12.308 482 2	14.157 772 7	14.499 435 9	14.655 292 6
k=11, resi.$< 3 \times 10^{-7}$	9.978 111 8	12.030 228 4	12.308 477 4	14.157 768 0	14.499 431 2	14.655 287 9

Table 3 The exponents (k) for the asymptotic tails, $\exp(kx)$, of the response functions and the occupied orbital, and their estimations of the H_2 (1.4 bohr) energies.

	exponent k	ε (hartree)[a]	$\varepsilon - \varepsilon_h$ (eV)[b]
$^1\Pi_g$	-0.307	-0.0471	14.9
$2^1\Sigma_g$	-0.274	-0.0375	15.2
$2^1\Sigma_u$	-0.288	-0.0415	15.1
$^1\Pi_u$	-0.468	-0.110	13.2
$1^1\Sigma_g$	-0.440	-0.0968	13.5
$1^1\Sigma_u$	-0.465	-0.108	13.2
HOMO	-1.11	-0.616	—

a) The relation $\exp(kx) = \exp(-\sqrt{-2\varepsilon}\,x)$ is used.
b) $\varepsilon_h = -0.5947$ (hartree) is used.

Table 4 The highest occupied orbital (ε_h) and the total energies (E;in hartree) of Be from the Hartree-Fock and LSDA calculations, with and without the asymptotic correction.

method	ε_h	E
HF (16s11p7d GTOs)[a]	-0.309 3	-14.572 9
LSDA (16s11p7d GTOs)[a]	-0.205 7	-14.447 1
LSDA/AC (16s11p7d GTOs)[a]	-0.307 7	-14.447 1
HF, k=7, resi.$< 1 \times 10^{-4}$	-0.309 27	-14.573 021
LSDA, k=7, resi.$< 1 \times 10^{-4}$	-0.205 73	-14.447 207
AC-LSDA, k=7, resi.$< 1 \times 10^{-4}$	-0.288 28	-14.444 828
Expt.[b]	-0.342 6	$\cdots$

a) Reference [18]
b) Reference [52]

Table 5 Excitation energies (in eV) of Be

	MADNESS k=7, resi.$< 1 \times 10^{-4}$			Hirata et al.[a] 16s11p7d GTOs			
State	CIS	LSDA	AC-LSDA	CIS	LSDA	LSDA/AC	Expt.[b]
^{1}S	7.265	5.608[e]	7.853[d]	7.26	5.66	7.20	8.09
^{3}S	7.101	5.605[d]	7.842[d]	7.10	5.64	7.12	8.00
^{1}D	7.573	5.64[c,e]	7.87[c,d]	7.58	⋯	7.52	7.99
^{3}D	6.839	5.62[c,d]	7.73[c]	6.84	5.83	6.83	7.69
^{1}P	6.775	5.609[e]	7.385	6.77	5.65	6.61	7.46
^{3}P	7.388	5.633[e]	7.860[d]	7.40	5.79	7.36	7.40
^{3}P	6.435	5.610[d]	7.302	6.44	5.65	6.41	7.30
^{1}D	6.921	5.62[c,d]	7.69[c]	6.92	5.83	6.75	7.05
^{1}S	6.131	5.586[d]	6.957	6.13	5.58	6.02	6.78
^{3}S	5.528	5.512	6.849	5.53	5.50	5.76	6.46
^{1}P	5.065	5.096	5.719	5.05	4.82	4.83	5.28
^{3}P	1.700	2.577	2.681	1.70	2.36	2.36	2.73

a) Reference [18]
b) Reference [53]
c) Degeneracies are obtained within 3 digits.
d) Unbound result. Residual and energy converged.
e) Unbound result. Residual did not converge, but energy did.

Table 6 The estimation of the singlet excitation and the highest occupied orbital energies from the asymptotic exponential tails of the response functions and the highest occupied orbital.

	CIS		LSDA		AC-LSDA	
	ε (hartree)	$\varepsilon - \varepsilon_h$ (eV)[a]	ε (hartree)	$\varepsilon - \varepsilon_h$ (eV)[a]	ε (hartree)	$\varepsilon - \varepsilon_h$ (eV)[a]
^{1}S	-0.0418	7.28	⋯	⋯	⋯	⋯
^{1}D	-0.0194	7.89	⋯	⋯	⋯	⋯
^{1}P	-0.0501	7.05	⋯	⋯	-0.0214	7.26
^{1}D	-0.0417	7.28	⋯	⋯	-0.00834	7.62
^{1}S	-0.0771	6.32	⋯	⋯	-0.0400	6.75
^{1}P	-0.125	5.02	-0.0234	4.96	-0.0885	5.44
HOMO	-0.299	—	-0.200	—	-0.281	—

a) The value of ε_h is as shown in Table 4.

Table 7 The highest occupied orbital energies (ε_h; in hartree) of N_2 (1.0980Å) for the Hartree-Fock and LSDA calculations, with and without the asymptotic correction.

method	ε_h
HF (6-311(3+,3+)G**)[a]	-0.635 5[c]
LSDA (6-311(3+,3+)G**)[a]	-0.384 1
LSDA/AC (6-311(3+,3+)G**)[a]	-0.611 8
HF, k=7, resi.$< 1 \times 10^{-4}$	-0.634 43[c]
LSDA, k=7, resi.$< 1 \times 10^{-4}$	-0.382 60
AC-LSDA, k=7, resi.$< 1 \times 10^{-4}$	-0.547 26
Expt.[b]	-0.572 6

a) Reference [18]
b) Reference [52]
c) The energy of the $3\sigma_g$ orbital.

Table 8 Vertical excitation energies (in eV) of N_2 (1.0980Å)

	MADNESS k=7, resi.$< 1 \times 10^{-4}$		Hirata et al.[a] 6-311(3+,3+)G**			
State	CIS	AC-LSDA	CIS	LSDA/AC	LSDA	Expt.[b]
$^1\Sigma_u^+$	14.306	13.888	14.37	13.25	10.70	12.98
$^1\Pi_u$	13.194	···	13.24	13.30	10.70	12.90
$^1\Sigma_g^+$	14.013	13.299	14.04	12.62	10.46	12.2
$^3\Sigma_g^+$	13.113	12.935	13.14	12.21	10.35	12.0
$^3\Pi_u$	11.721	10.504	11.81	10.42	10.36	11.19
$^1\Delta_u$	9.044	10.37[c]	9.04	10.34	10.26	10.27
$^1\Sigma_u^-$	8.495	9.768	8.47	9.76	9.70	9.92
$^3\Sigma_u^-$	8.494	9.768	8.47	9.76	9.70	9.67
$^1\Pi_g$	10.005	9.298	9.98	9.16	9.09	9.31
$^3\Delta_u$	7.293	8.96[c]	7.32	8.92	8.87	8.88
$^3\Pi_g$	7.992	7.651	8.02	7.62	7.58	8.04
$^3\Sigma_u^+$	6.225	8.159	6.20	7.94	7.91	7.75

a) Reference [18]
b) Reference [49]
c) Degeneracies are obtained within 3 digits.

Table 9 The highest occupied orbital energies (ε_h; in hartree) of H_2O (OH=0.9584Å, HOH=104.45°) for the Hartree-Fock and LSDA calculations, with and without the asymptotic correction.

method	ε_h
HF (6-311(3+,3+)G**)[a]	-0.510 0
LSDA (6-311(3+,3+)G**)[a]	-0.270 3
LSDA/AC (6-311(3+,3+)G**)[a]	-0.502 6
HF, k=7, resi.$< 1 \times 10^{-4}$	-0.510 56
LSDA, k=7, resi.$< 1 \times 10^{-4}$	-0.271 96
AC-LSDA, k=7, resi.$< 1 \times 10^{-4}$	-0.488 73
Expt.[b]	-0.463 8

a) Reference [18]
b) Reference [52]

Table 10 Vertical excitation energies (in eV) of H_2O (OH=0.9584Å, HOH=104.45°)

	MADNESS k=7, resi.$< 1 \times 10^{-4}$		Hirata et al.[a] 6-311(3+,3+)G**			
State	CIS	AC-LSDA	CIS	LSDA/AC	LSDA	Expt.[b]
$^1A_1$	11.465	12.198	11.49	11.04	8.52	10.17
$^1B_1$	11.163	11.822	11.26	10.81	7.49	10.0
$^3B_1$	11.036	11.707	11.15	10.77	7.48	···
$^1A_1$	10.897	10.176	10.88	10.00	7.72	9.67
$^3A_1$	10.718	···	10.80	10.71	8.18	···
$^1A_2$	10.360	10.187	10.32	9.81	7.48	9.1
$^3A_2$	10.013	9.862	9.97	9.60	7.48	···
$^3A_1$	10.105	11.413	10.07	9.47	7.70	···
$^1B_1$	8.695	8.059	8.64	7.97	6.50	7.4
$^3B_1$	8.019	7.515	7.97	7.53	6.24	7.2

a) Reference [18]
b) Reference [50]

Table 11 The highest occupied orbital energies (ε_h; in hartree) of C_2H_4 (CC=1.331Å, CH=1.081Å, CH=121.4°) for the Hartree-Fock and LSDA calculations, with and without the asymptotic correction.

method	ε_h
HF (d-aug-cc-pVTZ)[a]	-0.377 57
LSDA (d-aug-cc-pVTZ)[a]	-0.255 37
HF, k=7, resi.$< 1 \times 10^{-4}$	-0.377 71
LSDA, k=7, resi.$< 1 \times 10^{-4}$	-0.255 54
AC-LSDA, k=7, resi.$< 1 \times 10^{-4}$	-0.377 38
Expt.[b]	-0.386 37

a) Calculated with NWCHEM.
b) Reference[52]

Table 12 Vertical excitation energies (in eV) of C_2H_4 (CC=1.331Å, CH=1.081Å, CH=121.4°) for states formed by single excitations from $b_{3u} = \pi$ (molecule in the yz plane).

	MADNESS k=7, resi.$< 1 \times 10^{-4}$		NWCHEM d-aug-cc-pVTZ		
State	CIS	AC-LSDA	CIS	LSDA	Expt.[a]
$^1B_{1u}$	9.194	10.294	9.270	8.482	9.33
$^1B_{2u}$	8.779	9.598	8.929	8.251	9.05
$^1B_{3u}$	8.913	9.500	8.937	7.650	8.90
$^1B_{3u}$	8.589	9.093	8.840	7.354	8.62
$^3B_{3u}$	8.607	9.037	8.542	7.337	8.57
^1A_g	8.204	9.087	8.202	7.350	8.28
^3A_g	7.809	8.635	7.807	7.290	8.15
$^1B_{1u}$	8.364	8.889	8.362	7.639	8.0
$^1B_{2g}$	7.897	8.058	7.893	7.059	7.90
$^1B_{1g}$	7.740	8.033	7.737	7.072	7.80
$^3B_{1g}$	7.663	7.970	7.660	7.071	7.79
$^1B_{3u}$	7.161	7.316	7.158	6.632	7.11
$^3B_{3u}$	6.969	7.202	6.956	6.589	6.98
$^3B_{1u}$	3.792	4.864	3.794	4.860	4.36

a) Reference[51]

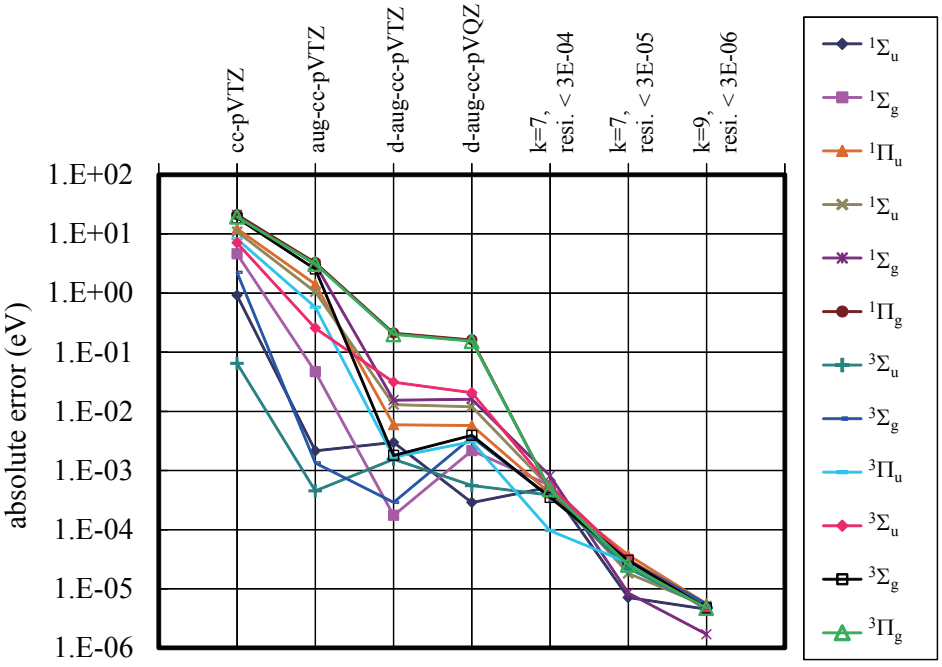

Fig. 1 The absolute errors of the CIS excitation energies of H_2 shown in Table 2. The error is defined as the difference between the CIS excitation energy and that calculated using the 11-th multiwavelet bases.

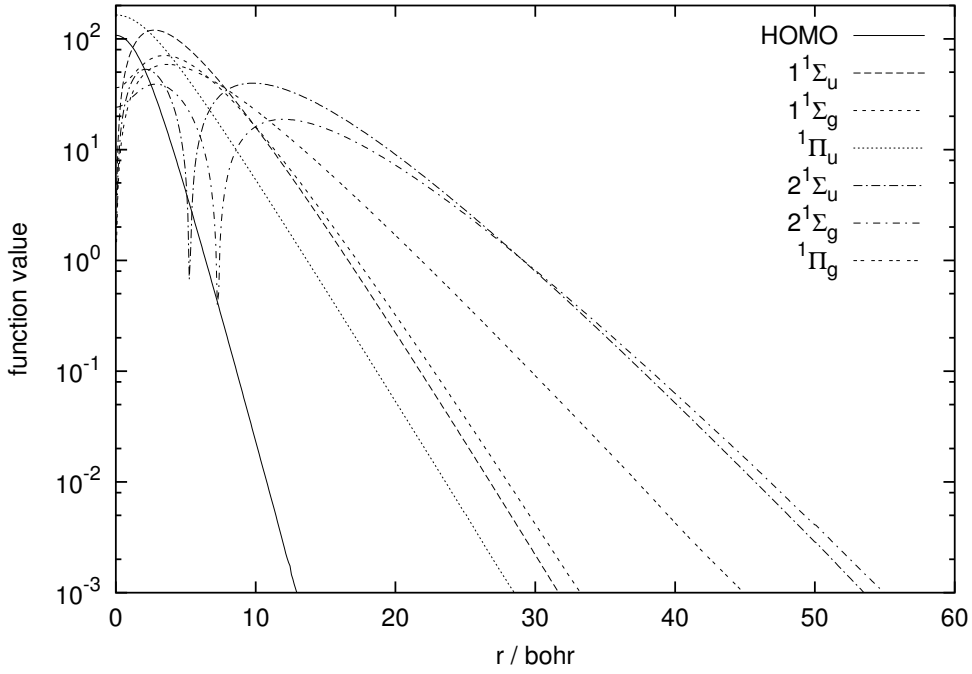

Fig. 2 Plots of the occupied orbitals and the response functions of the singlet excitations of H_2, as calculated with the HF-SCF and the CIS method using the 7-th multiwavelet bases. The plot axis is $(x, y) = (1.25, 0.0)$ in bohr.

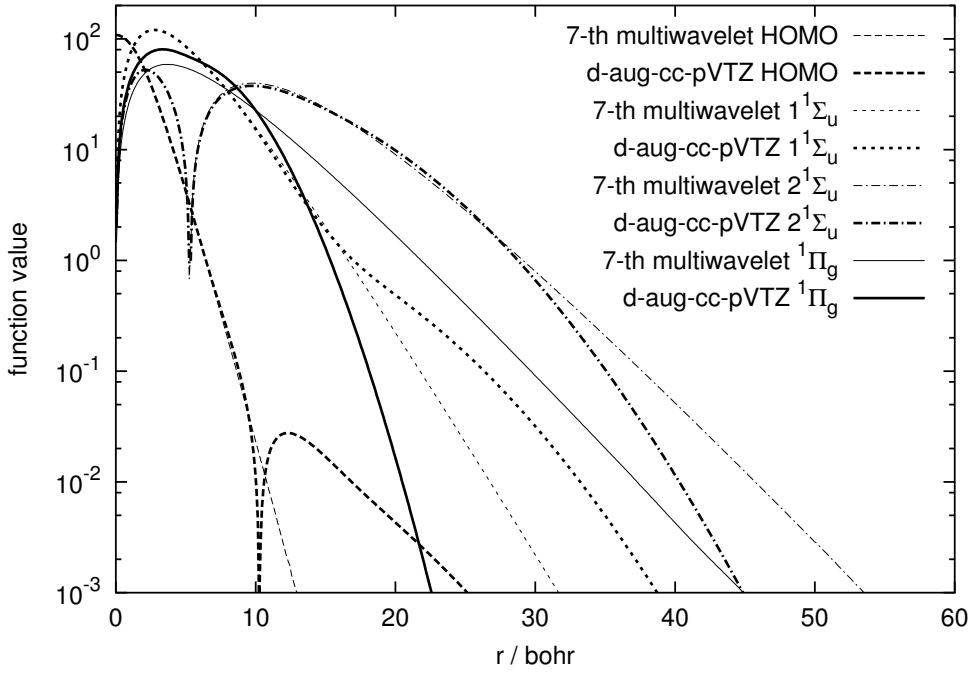

Fig. 3 Plots of the occupied orbital and the response functions of the singlet excitations, $1^1\Sigma_u$, $2^1\Sigma_u$, and $^1\Pi_g$ on H_2, as calculated by the HF and CIS methods using the d-aug-cc-pVTZ basis sets and the 7-th multiwavelet bases. The plot axis is $(x, y) = (1.25, 0.0)$ in bohr.

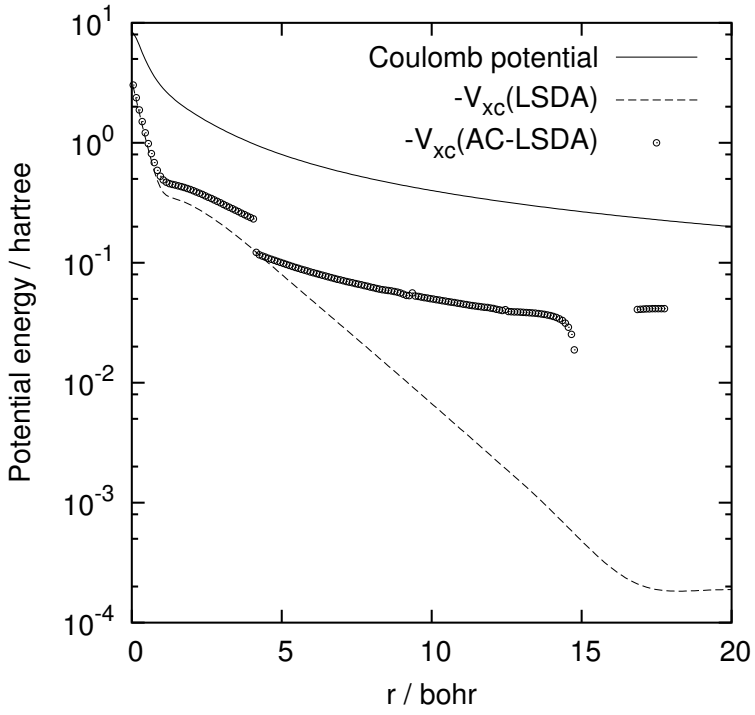

Fig. 4 Plots of the Coulomb potential and the exchange-correlation potentials of LSDA with and without the asymptotic correction for the Be atom; *r* indicates the distance from the nucleus.

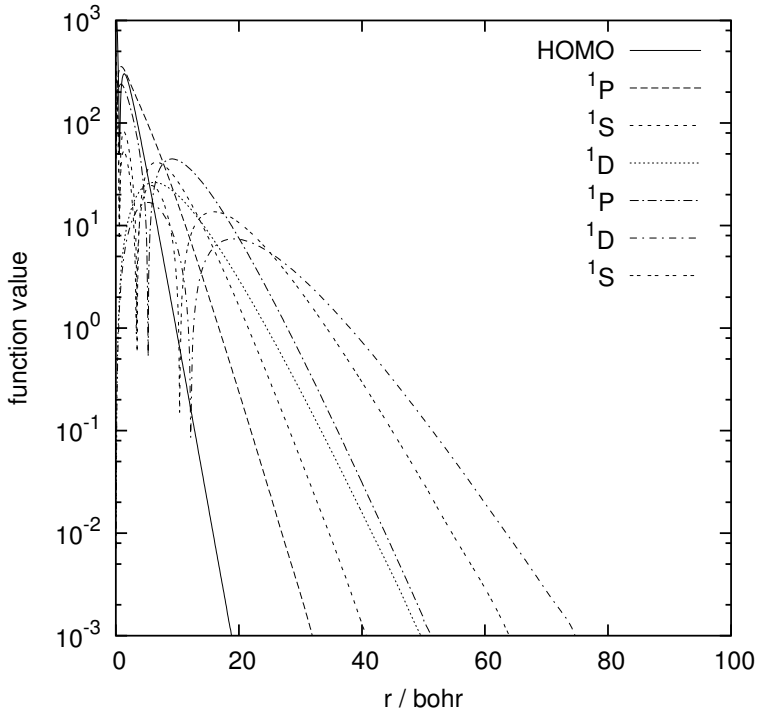

Fig. 5 Plots of the highest occupied orbitals and the response functions of the singlet excitations of Be, as calculated with the HF-SCF and CIS methods using the 7-th multiwavelet bases, along the z axis.

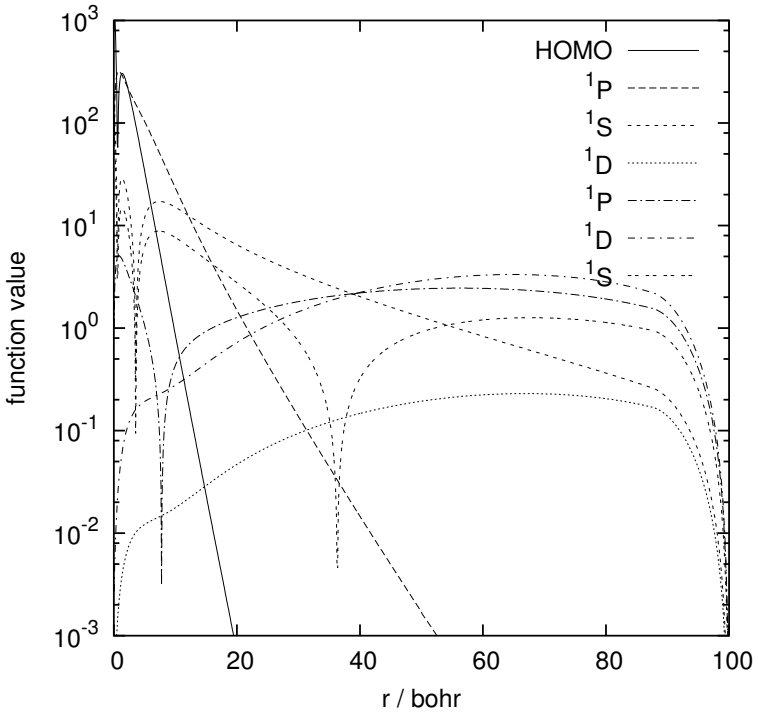

Fig. 6 Plots of the highest occupied orbitals and the response functions of the singlet excitations of Be, as calculated with LSDA exchange-correlation functional using the 7-th multiwavelet bases, along the z axis.

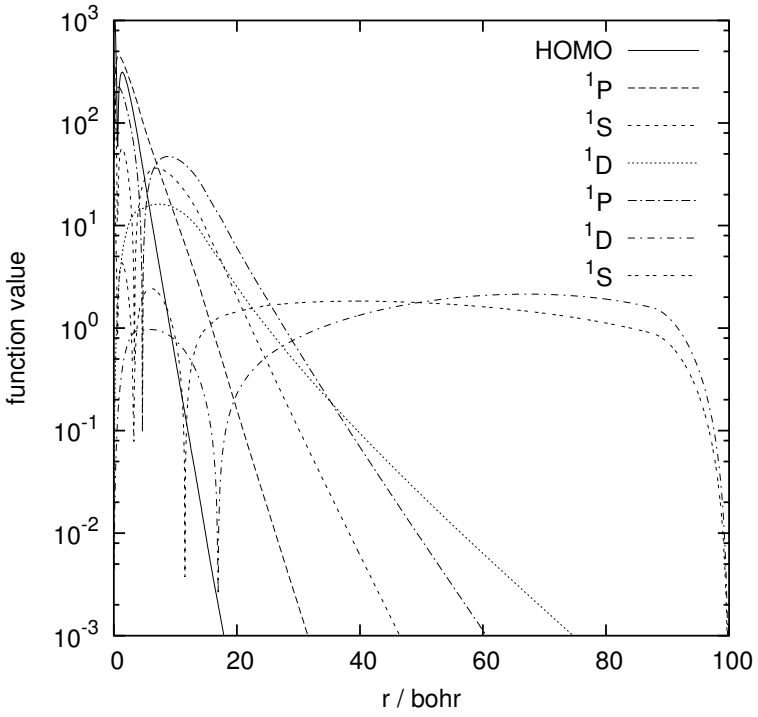

Fig. 7 Plots of the highest occupied orbitals and the response functions of the singlet excitations of Be, as calculated with the AC-LSDA exchange-correlation functional using the 7-th multiwavelet bases, along the z axis.